Science of the Total Environment 866 (2023) 161465

Contents lists available at ScienceDirect

Science of the Total Environment

journal homepage: www.elsevier.com/locate/scitotenv

Spatial–temporal evolution and driving force analysis of eco-quality in urban agglomerations in China

Lifang Zhang [a], Chuanglin Fang [a,b,*], Ruidong Zhao [a,c], Cong Zhu [a], Jingyun Guan [a]

[a] College of Geography and Remote sensing Sciences, Xinjiang University, Urumqi 830046, China
[b] Institute of Geographic Sciences and Natural Resources Research, Chinese Academy of Sciences, Beijing 100101, China
[c] School of Geography Science, Taiyuan Normal University, Jinzhong 030619, China

HIGHLIGHTS

- EQ's spatial and temporal evolution in China's urban agglomerations is analyzed.
- A GeoDetector model illustrates factors affecting the main drivers of EQ.
- The Hu-line reveals a spatial relationship in the distribution of EQ.
- EQ has improved in around 42 % of China's urban agglomerations.
- The driving forces of EQ in different urban agglomerations are spatially different.

GRAPHICAL ABSTRACT

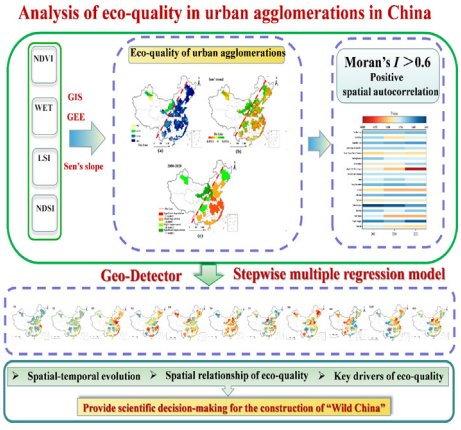

ARTICLE INFO

Editor: Martin Drews

Keywords:
Urban agglomerations
Ecological quality
GEE
Driving forces
GeoDetector
China

ABSTRACT

Urban agglomerations are important spatial carriers of regional economic development, and their ecological quality (EQ) is closely related to economic growth and human development. However, the rapid urbanization in China has generated a series of EQ problems that threaten the sustainable development of the country. Therefore, it is essential to explore changes in EQ for the development of sustainable "human–land" relations in urban agglomerations. Using GIS, GeoDetector, Stepwise multiple regression, and Sen'trend analysis, to reveal the spatial-temporal evolution of EQ in urban agglomerations along with the spatial heterogeneity of its driving forces in China. Results show that: (1) The annual change rate of EQ of urban agglomerations ranges from −0.0312 to 0.0334. Taking the Hu-line as a boundary, the EQ of urban agglomerations is spatially high in the east and low in the west. (2) The Global Moran's I index ranged from 0.740 to 0.687 during the study period, indicating a positive correlation in the EQ spatial distribution. The EQ of urban agglomerations has significant spatial agglomeration, with hot spots concentrated in the eastern region and cold spots in the northwestern region. (3) Main drivers of EQ of urban agglomerations are elevation, population density, nighttime light index, arable land area, real GDP per capita, precipitation, and built-up urban area ($q > 10$ %). (4) The stepwise multiple regression model spatially reveals that the nighttime light index, built-up urban area land and GDP per capita dominate the ecological quality changes of urban agglomerations, accounting for 73.68 % of the total number of urban agglomerations. This study provides an effective method for assessing spatial-temporal changes of EQ in urban agglomerations, supports scientific decision-making support for the construction of ecological civilization and the development of human–land harmony in urban agglomerations, and promotes the development and construction of "Beautiful China."

* Corresponding author at: College of Geography and Remote sensing Sciences, Xinjiang University, Urumqi 830046, China.
E-mail address: fangcl@igsnrr.ac.cn (C. Fang).

http://dx.doi.org/10.1016/j.scitotenv.2023.161465
Received 1 July 2022; Received in revised form 31 October 2022; Accepted 4 January 2023
Available online 7 January 2023
0048-9697/© 2023 Elsevier B.V. All rights reserved.

1. Introduction

Urban agglomerations are important carriers of economic accumulation, industrialization, and urbanization. From a global perspective, urban agglomerations have become an important carrier for the shift of the world's economic center of gravity and determine the future pattern of world economic development, and their status and role have become increasingly prominent (Fang and Yu, 2017). In the context of economic growth over recent decades, a contradiction in the process of urbanization and development has gradually emerged between the rapidly developing economy and ecological quality (EQ) (Dadashpoor et al., 2019; Fang et al., 2021). Therefore, it is important to emphasize the protection of urban ecology and improve the relationship between urban development and the ecological environment when building harmonious "human–land" coexistence. In China, ecology was emphasized in 1983 when ecological protection was incorporated into the basic state policy (Ministry of Ecology and Environment of the People's Republic of China, 2020), thus beginning an important chapter in the protection of the ecological environment in China. Since the 18th National Congress of China, there has been vigorous promotion of the construction of ecological civilization and ecological protection, the harmonious coexistence of humans and nature, and continuous improvement of EQ (The 18th National Congress of the Communist Party of China, 2012). China's 14th Five-Year Plan put forward higher requirements for the construction of ecological civilization (Ministry of Ecology and Environment of the People's Republic of China, 2020; Central People's Government of the People's Republic of China, 2021). The ability to promptly assess spatial and temporal changes in EQ is vital to the region's sustainable development. Thus, this research focuses on how to effectively build and evaluate EQ.

The ecological environment provides natural resources and living conditions for humans and is a prerequisite for human and social progress. EQ can reflect the strengths and weaknesses of the ecological environment, and its accurate evaluation can provide an important reference for solving regional ecological problems and promoting the sound development of society and ecology (Wang et al., 2019). Extant studies on EQ evaluation have used a range of methods, including the Driving–Pressure–State–Impact–Response (DPSIR) (Ke et al., 2021; Xu, 2013), Pressure-State-Response (PSR) (Xie et al., 2015), artificial neural network (Gebler et al., 2018), ecological footprint (Khan et al., 2021), Minimal Cumulative Resistance (MCR), and coupling coordination (Fang et al., 2016a; Fang and Ren, 2017) models. However, despite these methods' wide use, and the significant volume of research results obtained, the data have mainly been obtained from statistical yearbooks and the indicator construction has been deeply subjective, bringing various limitations for assessing large regions.

Since the 1970s, remote sensing (RS) has been widely used in EQ research because of its extensive coverage and data mapping, and its high efficiency, which can provide a deeper understanding of the dynamic processes within the world's land, oceans, and lower atmosphere (Avtar et al., 2020; Shao et al., 2020; Xu et al., 2021). The net primary productivity (NPP) of vegetation and the leaf area index (LAI) are relatively common ecological indices. Pan et al. (2021) extracted and dissected the response of NPP and LAI to environmental changes using RS images and determined the relationship between them. Land surface temperature (LST) plays a vital role in the analysis of surface biogeochemical processes as a key environmental parameter in the study of regional microclimates (Azmi et al., 2021; Subhanil et al., 2019), and has mainly been used to study topics such as urban climate change and urban morphology (Azmi et al., 2021; Lemoine-Rodríguez et al., 2022; Singh et al., 2017). Since vegetation is the main producer in the ecosystem, it is both time-consuming and labor-intensive to calculate vegetation cover artificially. Obtaining NDVI (on vegetation cover) from RS is a highly accurate way of assessing vegetation dynamics and generates significant savings in terms of human and material resources (Guo et al., 2018; Liu et al., 2022; Zhang et al., 2021b). The dryness index, also known as the normalized difference built-up index (NDBI), characterizes the urban building index and dryness to explain ecological conditions and is an important spectral index in RS imagery for which a significant correlation has been found with LST (Guha et al., 2018; Guha et al., 2021). The normalized difference water index (NDWI) is used to interpret the water content of vegetation and describes the physical changes associated therewith, which is important for ecological assessment and drought monitoring in arid areas (Ding et al., 2017). A series of studies have shown that RS satellite images are more reliable than field measurements (Abdulateef and Al-Alwan, 2020; El-Hattab et al., 2018).

While RS technology has yielded a significant volume of EQ monitoring research results, the following shortcomings remain. (1) The use of only one indicator to evaluate the state of EQ is insufficient due to the complexity and diversity of the natural environment. (2) Previous studies have relied primarily on the manual downloading and processing of RS data, not only resulting in a large workload and low error tolerance rate but also wasting a significant amount of research time. (3) The extant research has tended to focus more on evaluating indicators and spatial changes, along with the many driving factors that influence changes in EQ, with less focus on the driving mechanisms. In a bid to address the abovementioned shortcomings, a novel integrated RS ecological index is used to estimate the EQ of urban agglomerations. This is constructed in line with the approach used by Xu (2013), which involves combining greenness (NDVI), heat (LSI), NDBI, and humidity (WET), greatly compensating for the shortcomings of RS single-index evaluation (Shan et al., 2019). Meanwhile, an average value is used to circumvent these drawbacks to compensate for the instability of the data in the time series, as has previously been applied to a study of PM2.5 with positive results (Zhou et al., 2019). Moreover, the Google Earth Engine (GEE) big data platform hosts the Moderate-Resolution Imaging Spectroradiometer (MODIS), Landsat, and other massive RS data products, with powerful cloud computing and storage capabilities, thus effectively addressing the need for a mechanism with which to evaluate large areas, large scales, and long time series (Xiong et al., 2021). Finally, a geostatistical approach (the GeoDetector model) is used to detect the spatial heterogeneity of EQ and reveal the driving mechanisms. This approach has previously been applied to and yielded research results and recognition in areas such as disease, meteorology, economy, population, and nature (Luo et al., 2016; Wang and Xu, 2017; Wang et al., 2010).

In recent years, the characteristics and contradictions of urbanization and ecological environment in the process of regional development have attracted the attention of geographers. Naturally, EQ, with its strong applicability and scientific nature, has been widely used by scholars in the study of human-land relations. Boori et al. (2021) conducted an ecological vulnerability analysis of Russian cities based on the EQ, while Firozjaei et al. (2021) used the remote sensing index to quantify ecologically barren areas in Europe. Zhang et al., 2022 explored the evolution of the ecological environment and the driving factors in the Chang-Zhu-Tan urban area based on GEE's remote sensing ecological index. To date, domestic and foreign research on EQ has been limited to small regions such as economic zones or watersheds (Zheng et al., 2022), with a lack of research from a larger regional and global perspective. Meanwhile, the extant research on EQ has tended to focus on evaluation and spatial analysis and has failed to study its driving mechanisms in depth.

China is both the world's largest developing country and the center of future development and research on global urban agglomerations (Fang, 2019). Its level of urbanization increased from 7.30 % in 1949 to 59.58 % in 2018 (Yao et al., 2021), which is a remarkable achievement. However, its ecological environment has become more fragile alongside the development of urbanization and industrialization, giving rise to a series of environmental pollution problems. The need to address the contradiction between economic development and ecological protection has thus become even more pressing, and has led to widespread concern over ecological issues (Fang et al., 2016a; Fang et al., 2017). Urbanization level has been used as an important indicator for studying regional ecological security, ecosystem services, ecological risk, and EQ (Qiu et al., 2021; Tang et al., 2021; Wang et al., 2022). China's 14th Five-Year Plan clearly states that the continuous improvement of environmental quality is vital to promote

ecological civilization and ensure China remains beautiful (National Development and Reform Commission, 2021). Therefore, timely monitoring and evaluation of the EQ of urban agglomerations is of great practical significance in terms of realizing the high-quality development of China's urban agglomerations.

This study aims to answer the question, "What are the spatial and temporal characteristics of EQ of Chinese urban agglomerations at different scales over the past 20 years? What are the mechanisms driving the EQ of different urban agglomerations? Is it natural factors or human activities that dominate the EQ of urban clusters? What is the role of human activities in improving or worsening the EQ of urban agglomerations? There are no clear answers to the above questions. In this study, we use different models to try to step out a parameter, or a smaller set of runs, to find out the sensitivity of the driving factors, and seek the sensitivity of human activities for different urban clusters under the assumption that they are not influenced by natural conditions. It is against this background that it has become necessary to monitor spatial and temporal changes in the EQ of China's urban agglomerations, explore their spatial evolution characteristics, attempt to identify the main driving factors, and provide a scientific basis for the development of sustainable decision-making. The main objectives of the study are therefore as follows:

(1) To evaluate and monitor the spatial–temporal changes of EQ in 19 urban agglomerations in China from 2000 to 2020.

(2) To explore the spatial differentiation and spatial correlation characteristics of EQ of urban agglomerations in China.

(3) To uncover the mechanisms driving the EQ of urban agglomerations in China.

Based on the GEE and GIS platform, this study combines RS imagery, land use data, and meteorological and socioeconomic data to construct EQ indicators, analyze the EQ changes and spatial differentiation characteristics of urban agglomerations, and apply the GeoDetector model and stepwise multiple regression model to identify factors of EQ in urban agglomerations to gain comprehensive insights into the drivers of EQ, with a view to actively promoting the construction of ecological civilization in urban agglomerations in China, realizing human–land harmony, and providing a scientific basis and theoretical guidance for the construction of a "Beautiful China."

2. Study area and data sources

2.1. Introduction to the study area

The study area comprises the 19 urban agglomerations of China proposed in the National New-type Urbanization Plan (2014–2020) (Fig. 1). These are made up of five national-level urban agglomerations (the Beijing–Tianjin–Hebei, Yangtze River Delta, Pearl River Delta, Middle Reaches of Yangtze River, and Chengdu–Chongqing urban agglomeration), eight regional, medium-sized urban agglomerations (Central and southern Liaoning, Shandong Peninsula, West Coast, Harbin–Changchun, Central Plains, Guanzhong, and Beibu Gulf urban agglomerations, plus the urban agglomeration on the northern slope of the Tianshan Mountains), and six local, small urban agglomerations (the Jinzhong, Hubao–Egyu, Central Yunnan, Central Guizhou, and Lanxi urban agglomerations, plus the urban agglomeration along the Yellow River in Ningxia) (Fang et al., 2021; Fang et al., 2015). While the population and economic clustering role of urban agglomerations continued to emerge up to the end of 2019, these 19 urban agglomerations account for around 25 % of the land area in China, support >75 % of the country's urban population, and contribute >80 % of China's GDP.

2.2. Data sources and preprocessing

The research data mainly include MODIS RS image data, land use data, air quality data, meteorological data, and socioeconomic data (Fig. 2), which are described as follows:

(1) RS data: MODIS series RS images are used to construct the long-term series of EQ index (2000 − 2020). The four ecological components (NDVI, WET, LST, and NDBI) based on the GEE cloud platform were selected

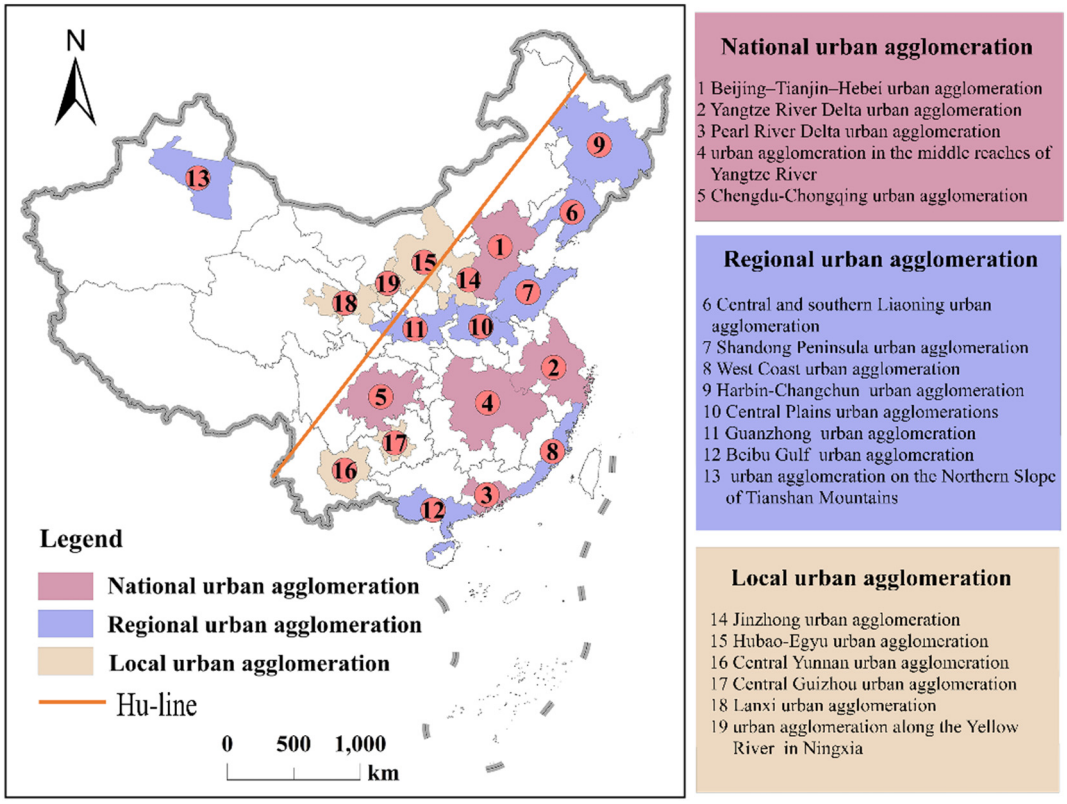

Fig. 1. Schematic diagram of China's urban agglomeration planning area.

Name	Description	Source
Land-use data	30 m resolution	The 30 m annual land cover datasets and its dynamics in China from 1990 to 2020 (https://zenodo.org/record/5210928).
Remote-sensing image	MODIS 13A1, MOD11A2, MOD09A1	National Aeronautics and Space Administration (NASA) (https://earthdata.nasa.gov/)
DEM	90 m resolution	National Geospatial Data Cloud (http://www.gscloud.cn/)
PM 2.5	Unit:： mg/m³	National Earth System Science Data Center, National Science & Technology Infrastructure of China (http://www.geodata.cn)
CO_2	Unit: 10^8kg	All emission inventories are compiled based on latest energy data revision (2015) by Chinese Statistics Bureau.
Precipitation	Unit:1 mm	Annual precipitation data with 1km resolution in China (2001-2020); Monthly mean temperature dataset with 1km resolution in China from 1901 to 2020; National Science and Technology Infrastructure Platform—National Earth System Science data (http://www.geodata.cn).
Temperature	Unit:1°C	
Nighttime light data	——	An extended time series of cross-sensor calibrated global NPP-VIIRS nighttime light data (2000–2021)
Population density	Unit:100 m	Pop published by the WorldPop project and has a spatial resolution of 100 m(2000-2020) (https: //wopr.worldpop.org.uk)
Real GDP per capita	GDP of a nation/population	China Urban Statistical Yearbook (2000-2020), China Urban Construction Statistical Yearbook (2000-2020), National Economic and Social Development Statistical Bulletin, some missing data combined with corresponding provincial and municipal (autonomous regions), local and municipal data to supplement
Urbanization level	Urban Population/ Total Resident Population (%)	

Fig. 2. Research data sources.

from the NASA (https://earthdata.nasa.gov/) MODIS product library as the data source for the July–September period for each year of study. NDVI is derived from the MOD13A1 V6 dataset, LST from the MOD11A2 V6 dataset, and WET and NDBI from the MOD09A1 dataset. To ensure the reliability and smoothness of the EQ, the data were averaged over three years, with the intermediate years used as the basis for the study data. For example, the EQ of the urban agglomerations in 2010 is the summed average of the EQ values for 2009, 2010, and 2011.

(2) Socioeconomic data: The nighttime light indices were sourced from an extended time series of cross-sensor calibrated global NPP-VIIRS nighttime light data (2000 − 2021) (Chen et al., 2021). Population density data (2000–2020) were sourced from WorldPop data published by the Geodata Institute, University of Southampton, UK. Real GDP per capita (2000–2020) and urbanization level data (2000–2020) were calculated from regional statistical yearbooks (National Bureau of Statistics of China (NBS): http://www.stats.gov.cn/) and national economic and social development statistical bulletins, with various missing data supplemented using more recent years.

(3) Other data: Land use data (2000–2020) were used to extract the arable land and built-up urban area of the urban agglomerations from the 30 m annual land cover datasets and its dynamics in China from 1990 to 2020 (Yang and Huang, 2021) (https://zenodo.org/record/5210928). Elevation data were obtained from the National Geospatial Data Cloud (http://www.gscloud.cn/) to extract elevation factors with a resolution of 90 m. Air quality data including PM 2.5 (2000–2020) (particulate matter 2.5)and CO_2(carbon dioxide)were obtained from National Earth System Science Data Center, National Science & Technology Infrastructure of China (http://www.geodata.cn) (Wei et al., 2021) and the results of Shan et al. (2020), respectively. Meteorological data, including annual average precipitation (2001 − 2020) and temperature data (2000–2020) (Peng et al., 2019), were obtained from the National Data Center for Earth System Science & Technology Infrastructure of China (http://www.geodata.cn), a national science and technology infrastructure platform, through raster conversion and processing by GIS software.

3. Methodology

3.1. EQ index construction

The four ecological indicators of greenness, wetness, heat and dryness are intimately connected with EQ (Zhang et al., 2022). Therefore, using the GEE platform, the MODIS data required to integrate the four important indicators reflecting the EQ index (NDVI, WET, LST, and NDBSI represent green, wet, hot and dry, respectively). They synthesize the EQ conditions of the area (Xu, 2013) through the following equation and steps (Fig. 3):

$$RSEI = PCA[f(NDVI, WET, LST, NDBSI)] \tag{1}$$

$$Wet = C_1\rho_{\text{red}} + C_2\rho_{\text{nir1}} + C_3\rho_{\text{blue}} + C_4\rho_{\text{green}} + C_5\rho_{nir2} + C_6\rho_{swir1} + C_7\rho_{swir2} \tag{2}$$

$$NDBSI = \frac{IBI + BI}{2} \tag{3}$$

$$IBI = \frac{\frac{2\rho_{swir1}}{2\rho_{swir1}+\rho_{nir1}} - \left[\frac{\rho_{nir1}}{\rho_{nir1}+\rho_{red}} + \rho_{green}/\left(\rho_{green}+\rho_{swir1}\right)\right]}{\frac{2\rho_{swir1}}{2\rho_{swir1}+\rho_{nir1}} + \left[\frac{\rho_{nir1}}{\rho_{nir1}+\rho_{red}} + \rho_{green}/\left(\rho_{green}+\rho_{swir1}\right)\right]} \tag{4}$$

$$BI = \frac{[(\rho_{swir1}+\rho_{red}) - (\rho_{nir1}+\rho_{blue})]}{[(\rho_{swir1}+\rho_{red}) + (\rho_{nir1}+\rho_{blue})]} \tag{5}$$

where *NDVI* denotes greenness, considering the saturation problem of NDVI in areas with high vegetation coverage, and EVI is used as the green component. Since the MOD13A1 V6 image set already contained the EVI layer, there was no need to calculate the EVI separately, the data were synthesized at a spatial resolution of 500 m, using the best pixels over a 16-day period (Zheng et al., 2020). *WET* denotes wetness, where ρ_{red}, ρ_{nir1}, ρ_{blue}, ρ_{green}, ρ_{nir2}, ρ_{swir1}, and ρ_{swir2} represent the reflectance of the seven bands of MOD09A1 images (Zhang et al., 2002). The coefficients of the respective bands of the multiband MODIS images are as follows: c = 0.11471, c = 0.24892, c = 0.24083, c = 0.31324, c = −0.31225, c = −0.64166, and c = −0.50877 (Xu et al., 2019). *LST* denotes heat, and the heat component was derived from the DLST layer of the MOD11A2 V6 dataset, providing an 8-day average land surface temperature at 1 km spatial resolution. As in previous studies, the third component of the k-t-transformed multispectral images was used to characterize the wetness component of *RSEI* (Todd and Hoffer, 1998). *NDSI* denotes dryness. The normalized difference build-up and soil index (NDBSI) was constructed based on the bare soil index (Hu and Xu, 2018; Rikimaru et al., 2002) and the index-based built-up index (IBI) (Xu, 2008), where ρ_{red}, ρ_{blue}, ρ_{green}, ρ_{nir1}, and ρ_{swir1} represent the surface reflectance of the corresponding bands in the

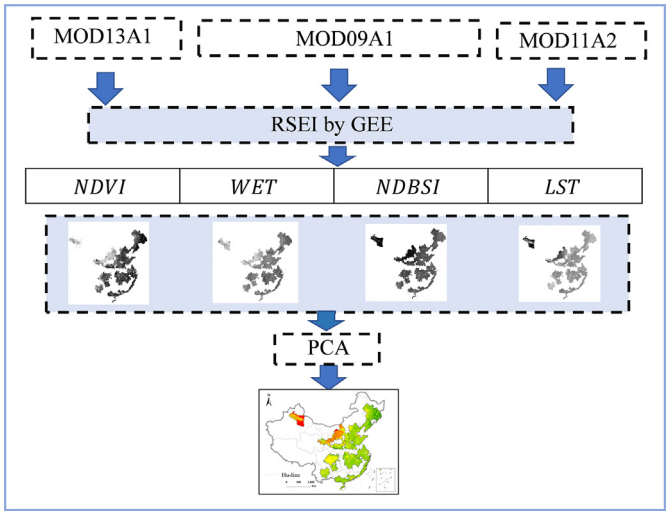

Fig. 3. Technical framework.

MOD09A1 V6 images. Principal component analysis was used to determine the weighting method, and any inconsistency between the indicator scales was eliminated through normalization. When the *RSEI* is close to 1 the EQ is considered to be high, and low when it is close to 0.

3.2. Spatial agglomeration analysis method

Spatial autocorrelation analysis refers to the geospatial correlation of the attribute values of a study object caused by its geographical order or location. The spatial correlation of EQ can be further explored in different spatial and temporal contexts, thus giving it strong academic research value in terms of exploring its intrinsic laws. For this reason, academics usually adopt spatial autocorrelation methods to study the spatial clustering and change patterns of EQ.

3.2.1. Spatial autocorrelation analysis

The Global Moran's *I* index tests the global spatial autocorrelation of EQ. A Moran's *I* index that is >0 indicates a positive correlation, with larger values indicating greater spatial agglomeration of EQ. A Moran's *I* index of <0 shows a negative spatial correlation, with smaller values indicating greater spatial dispersion of EQ. The formula is as follows (Anselin, 1995; Cliff and Ord, 1982; Moran, 1950):

$$I = \frac{n}{S_O} \times \frac{\sum_{i=1}^{n}\sum_{j=1}^{n} W_{ij} Z_i Z_j}{\sum_{i=1}^{n} Z_i^2},\ S_O = \Sigma_{i=1}^{n}\Sigma_{j=1}^{n} W_{ij},\ Z_i = Y_i - \overline{Y}, Z_j = Y_j - \overline{Y} \tag{6}$$

where I is the global spatial autocorrelation index, Y_i and Y_j are the observed air quality values of i and j, respectively, with $\overline{Y}$ as the mean value, and W_{ij} is the spatial weight matrix, usually taken to be 1 for adjacent cells and 0 for others. $I \in [-1, 1]$; when $I \in [-1, 0]$, it indicates a negative correlation between regional units. n is the number of study units; when $I = 0$, it indicates no correlation between regional units, and when $I \in [0, 1]$, it indicates a positive correlation between regional units. A Moran's *I* index closer to 1 indicates a closer relationship between the attribute values of the regional units; a value closer to 0 indicates that the attribute values are not correlated between the regional units; and a value closer to -1 indicates a greater difference in the attribute values between the units.

3.2.2. Hot-spot analysis (Getis-Ord Gi*)

Hot-spot analysis measures local autocorrelation characteristics that identify high and low EQ clusters in urban agglomerations. The high and low values of the Getis-Ord Gi* index measure the local clustering of cold and hot spots in the spatial pattern of EQ in urban agglomerations (Getis and Ord, 1996). The formula is as follows.

$$G_i^*(d) = \Sigma_{j=1}^{n} W_{ij}(d) X_j / \Sigma_{j=1}^{n} X_j \tag{7}$$

$$Z(G_i^*) = \left[G_i^* - E(G_i^*)\right] / \sqrt{VAR(G_i^*)} \tag{8}$$

where $G_i^*(d)$ is the statistic of each spatial unit i based on the spatial distance weight $W_{ij}(d)$, and $Z(G_i^*)$ is the standardized statistic of the $G_i^*(d)$ test—if the value is significantly positive, it indicates a hot-spot cluster, and vice versa, a cold-spot cluster. X_j is the attribute value of spatial unit j. $E(G_i^*)$ and $VAR(G_i^*)$ are the mathematical expectation and coefficient of variation of $G_i^*(d)$, respectively.

3.3. The estimation of Sen's slope

Sen's slope method utilizes the median of a sequence to identify a trend, and this approach can, to a certain extent eliminate the influence of data anomalies in trend tests and reduce noise interference (Sen, 1968). The calculation formula is as follows:

$$\beta = Median\left(\frac{x_j - x_i}{j - i}\right), \forall j > i \tag{9}$$

where x_i and x_j represent the data values ($j > i$) at times i and j, respectively. The trend degree β is used to judge the rise and fall of the time series trend. When $\beta > 0$, the time series shows an upward trend; otherwise, it shows a downward trend.

The Mann–Kendall (M–K) significance test is generally combined with Sen's slope method to complete the significance test of sequence trends (Mann, 1945; Gocic and Trajkovic, 2013). The formulas are as follows:

$$Z = \begin{cases} \dfrac{S}{\sqrt{Var(S)}} & (S > 0) \\ 0 & (S = 0) \\ \dfrac{S+1}{\sqrt{Var(S)}} & (S < 0) \end{cases} \tag{10}$$

$$S = \Sigma_{i=1}^{n-1}\Sigma_{i=1}^{n}\ sgn(x_j - x_i) \tag{11}$$

$$Var(S) = \frac{n(n-1)(2n+5)}{18} \tag{12}$$

$$sgn(x_j - x_i) = \begin{cases} 1 & x_j - x_i > 0 \\ 0 & x_j - x_i = 0 \\ -1 & x_j - x_i < 0 \end{cases} \tag{13}$$

where n represents the length of the time series, xj and xi are the data values at times j and i ($j > i$), respectively, and sgn ($xj - xi$) is the symbolic function. Under a set significance level α of, $|Z| > u1 - \alpha/2$ represents a significant change in the time series. When $|Z|$ is >1.65, 1.96, and 2.58, it means that the time series has passed the significance test at 90 %, 95 %, and 99 % probability, respectively. The method is calculated in MATLAB software.

3.4. GeoDetector

The mechanisms that drive the spatial and temporal evolution of EQ in urban agglomerations are multifaceted and can be scientifically and rationally detected using a GeoDetector model. Wang et al. (2010) demonstrated that GeoDetector can directly detect the magnitude of the driving factors in the distribution of EQ. Therefore, in this paper, the GeoDetector's factor detection method is used to investigate the magnitude of the

explanatory power of each factor on EQ. The factor detection equation is as follows:

$$q = 1 - \frac{\sum_{h=1}^{L} N_h \sigma_h{}^2}{N\sigma^2} \quad (14)$$

where q denotes the explanatory strength of a factor on the spatial and temporal distribution of EQ, with a value range of [0,1], $h = 1, \ldots, L$ is the number of levels of EQ impact factor, N_h and N are the number of samples of EQ influence for factor level h and the study area, respectively, and σ_h and σ are the variance of EQ values of level h and the whole study area, respectively. In the results, the higher the q-value of a factor, the stronger the explanatory power of that factor on the EQ of the study area. A factor with $q = 0$ has no relationship with the distribution of EQ in the study area. When $q = 1$, the factor completely controls the distribution of EQ in the study area. q takes values in the range [0,1], and the larger the value of q, the greater the driving effect of factor q on EQ.

3.5. Stepwise multiple regression model

A multiple stepwise regression model was used to analyze the main drivers affecting the EQ of China's urban agglomerations. The ultimately identified regression and predictor variables are shown by Eq. (15):

$$EQ \sim P1 + P2 + P3 + P4 + P5 \quad (15)$$

where P1 represents the Nighttime light index; P2, P3,P4 and P5 represent the Arable land area, Population density, GDP per capita, and Built-up urban area. This study used the LMG model to measure the relative importance of different drivers to the EQ change in China's urban agglomerations. The LMG model was bootstrapped using1000 replicates, yielding a 95 % confidence interval. This method uses the R package “relaimpo” for calculations (Gocic and Trajkovic, 2013; Groemping, 2006).

4. Results and analysis

4.1. Spatial–temporal variation characteristics of EQ of urban agglomerations in time series

From the spatial pattern of the annual average ecological quality from 2000 to 2020 (Fig. 4a), the ecological quality of China's urban agglomerations is generally bounded by the Hu-line, with a general trend of higher in the east and lower in the west. From the multi-year EQ averages, the high values (>0.6) are concentrated in the northeastern and eastern coastal urban agglomerations of China, the urban agglomerations with EQ averages between 0.4 and 0.6 are mainly located in the southern part of China, and the areas with EQ averages between 0.2 and 0.4 are mainly located in the western urban agglomerations of the Hu Huanyong Line. the lowest EQ averages (<0.2) are located in the urban agglomerations of the northern slopes of the Tianshan Mountains in northwestern China, which are characterized by arid climate and sparse vegetation. The region is characterized by arid climate and sparse vegetation.

The results of Sen's slope method analysis can reflect the trend of EQ change more effectively (Fig. 4b). The trend of EQ variation obtained based on Sen's slope method shows that the annual variation rate of EQ of urban agglomerations ranges from −0.0312 to 0.0334. In the recent 21 years, the EQ changes of 19 urban agglomerations in China are clearly bounded by the Hu-line, with the west side of the line mainly in an improved state and the east side in a deteriorated state. The trend pattern of EQ time series from 2000 to 2020 has a significant spatial heterogeneity (Fig. 4c), with about 42.11 % of urban agglomerations showing an improving trend and 21.05 % showing a significant improving trend ($p < 0.05$) (e.g. Lanxi, Hubao-Yueyu urban agglomerations, etc.). These regions are mainly located in the central and northwestern urban agglomerations of China. About 57.79 % of the urban agglomerations showed deterioration, and 21.05 % showed significant deterioration ($p < 0.05$) (e.g. Central Plains, Yangtze River Delta, Middle Reaches of Yangtze River urban agglomerations, etc.), with significantly deteriorated urban agglomerations mainly located in the eastern and southeastern coastal urban agglomerations, which generally have higher EQ values.

4.2. Spatial–temporal analysis of EQ in urban agglomerations for 2000, 2010 and 2020

To further understand the development stages and spatial characteristics of EQ of urban agglomerations, we analyzed the spatial and temporal changes of EQ of urban agglomerations by stages and different scales in three periods of 2000, 2010 and 2020, respectively (Fig. 5).

(1) From the pixel scale, the highest EQ pixel values were 0.929, 0.907, and 0.865, in 2000, 2010, and 2020, respectively, while an optimal state was found for 2010 (Fig. 5a). The mean values from 2000, 2010, and 2020 were 0.599, 0.601, and 0.598, respectively. The lowest values in 2000, 2010, and 2020 were 0.039, 0.008, and 0.033, respectively.

(2) On the municipal scale, cities with better EQ are mainly located in Jilin Province in northeastern China, while cities with lower EQ are generally located in the northwestern arid zone, such as the cities of Turpan, Changji, and Urumqi. Eighty percent of cities recorded an improved EQ from 2000 to 2020, with the most noticeable improvement in Kuitun, Zhoushan, Qinzhou, and Lanzhou (Fig. 5b). The remaining 20 % of cities saw a deterioration in EQ, of which Zhengzhou, Ziyang, and Tianmen are the most obvious.

(3) From the scale of urban agglomerations, the regions with lower EQ are mainly regional-level and local urban agglomerations, while the national-level urban agglomerations have a relatively positive EQ (Fig. 5c). Taking the Hu-line as a boundary, it is found that the eastern urban agglomerations have a generally higher EQ, including the Harbin–Changchun, central and southern Liaoning, and Jinzhong urban agglomerations. In contrast, the urban agglomerations on the west side of the Hu-line have a relatively low EQ. This can be attributed mainly to the fact that the region is located in the northwest of China, far inland, with little precipitation, low vegetation coverage, and a sensitive ecological environment. Over the study period, the EQ of the urban agglomerations tended to improve (most obviously in the urban agglomeration along the Yellow River in Ningxia, and the Hubao–Egyu and Lanxi urban agglomerations), except for the Central Plains, Central Guizhou, and Central Yunnan urban agglomerations, which showed a slight decline.

In summary, different scales were used to carry out the spatial and temporal analysis of EQ over three periods in the Chinese urban agglomerations. Taking the Hu-line as a boundary in spatial distribution, the EQ of the eastern urban agglomerations is relatively better than that of the agglomerations on the western side, with the high EQ values found mainly in the Harbin–Changchun, central and southern Liaoning, Jinzhong, Beijing–Tianjin–Hebei, and Beibu Gulf urban agglomerations. The analysis of changes in EQ shows that the most obvious improvement is in the urban agglomeration located on the Loess Plateau, indicating that the ecological restoration (Yurui et al., 2021) and soil and water conservation measures such as returning farmland to the forest (and grass), afforestation, and wind and sand control have achieved visible results in this region.

4.3. Spatial agglomeration effect of EQ

4.3.1. Moran's I analysis

To further understand the spatial correlation of EQ in urban agglomerations, the GeoDa spatial statistics tool was used to test the spatial autocorrelation and cluster analysis of EQ in China's urban agglomerations in 2000, 2010, and 2020. Consequently, the Moran's I index was found to be positive and above 0.65 for all of the urban agglomerations. In addition, all passed the significance test at the 1 % level, thus indicating the existence of significant spatial autocorrelation of EQ in the urban agglomerations. Fig. 6 shows Moran's I index scores for 2000, 2010, and 2020 of 0.7403, 0.7074, and 0.6878, respectively, with the scatter points mainly distributed in the first and third quadrants, thus indicating that the EQ of the urban

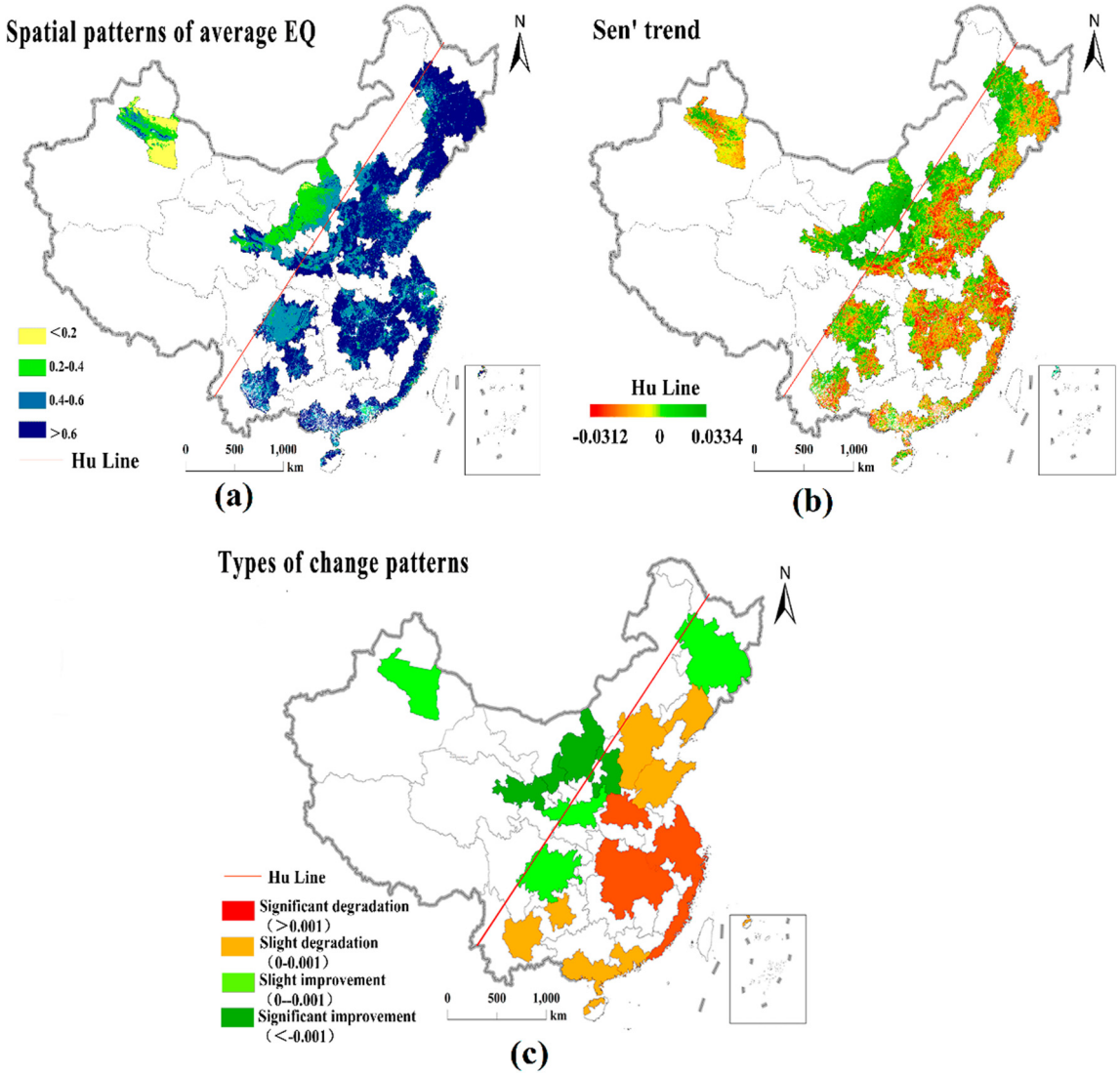

Fig. 4. Changes in EQ from 2000 to 2020.

agglomerations in China has a strong positive spatial correlation and significant spatial clustering characteristics.

Spatial autocorrelation tests on individual city groups (Fig. 7) revealed that the Moran's *I* index showed significant differences across years and urban agglomerations, and almost all of them pass the significance test. High Moran's *I* index scores were mainly found in the Harbin–Changchun, Chengdu–Chongqing, Beijing-Tianjin-Hebei, Central and southern Liaoning, Shandong Peninsula, Central Changjiang River, and the Yangtze River Delta urban agglomerations, which had significant agglomerations of EQ. Lower Moran's *I* index scores were seen mainly in the Hubao–Egyu, Jinzhong, Pearl River Delta, and Central Guizhou urban agglomerations. Overall, the spatial agglomeration of each urban agglomerations generally shows an increasing trend.

4.3.2. Analysis of spatial agglomeration

The spatial correlation characteristics of EQ in China's urban agglomerations were determined from the above macroscopic analysis, and the Getis-Ord Gi* index was used to depict the evolution trends of EQ cold and hot spots, which can be used to further analyze whether EQ is spatially heterogeneous at the local scale. Overall, Fig. 8 shows some apparent characteristics of the division between the hot and cold spots of EQ in China's urban agglomerations, using the Hu-line as a boundary. The urban agglomeration on the northern slope of the Tianshan Mountains, the Hubao–Egyu urban agglomeration, the urban agglomeration along the Yellow River in Ningxia, Chengdu-Chongqing urban agglomeration, and the Lanxi urban agglomeration on the west side are generally cold-spot areas, indicating that the urban agglomerations in this region have a poor EQ. The hot spots on the eastern side of the Hu-line are concentrated in central China (Jinzhong and Central Plains urban agglomeration, etc.) and in the northeast (Central and southern Liaoning and Harbin–Changchun urban agglomerations). Since 2000, the share of cities in the hot spots has continued to fall, while the percentage of cold spots has continued to rise. During the study period, there was a gradual weakening of hot spots in areas such as the Central Plains, Jinzhong, and Guanzhong urban agglomerations, and the EQ gradually deteriorated; at the same time, there was a gradual weakening of cold spots in areas such as the Pearl River Delta and the West Coast urban agglomerations, and the EQ improved.

4.4. Analysis of driving factors of EQ

4.4.1. Indicator selection

To explore the mechanisms underlying the spatial and temporal heterogeneity of EQ in China's urban agglomerations, it is necessary to focus on the main drivers of EQ heterogeneity and the similarities and differences in the drivers of EQ across time and regions. The spatio-temporal evolution of EQ is a relatively complex process. Considering that the EQ of urban

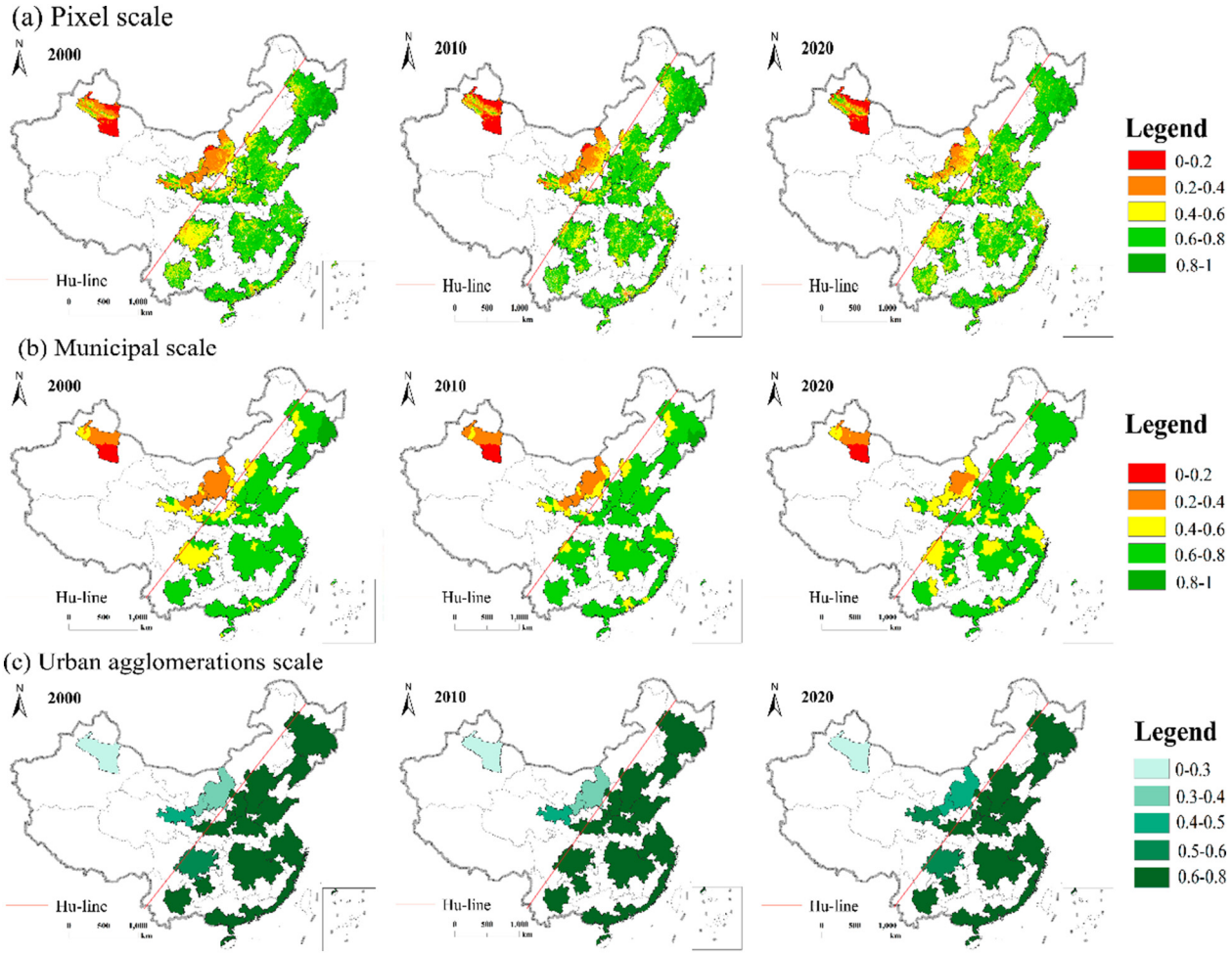

Fig. 5. Spatial distribution of EQ at different scales in 2000, 2010, and 2020.

agglomerations is influenced by various factors, this study mainly selects the following 11 detection factors—Nighttime light index (X1), Population density (X2), Temperature (X3), Precipitation (X4), Arable land area (X5), Urbanization level (X6), Real GDP per capita (X7), PM2.5 (X8), Elevation (X9), Built-up urban area (X10), and CO_2 (X11)—for the detection analysis of factors that drive EQ. First, using the GIS platform, the urban agglomerations were sampled uniformly, with 233 sampling points. Second, the 11 detection factors were discretized and categorized using reclassification tools (Fig. 9) and then imported into the GeoDetector model for calculation.

4.4.2. Factor detection results of GeoDetector

The GeoDetector model was used to detect the EQ driver q for the urban agglomerations, with a higher q-value indicating a greater driver of EQ. The model thus measured the q-values of each detection factor's ability to drive

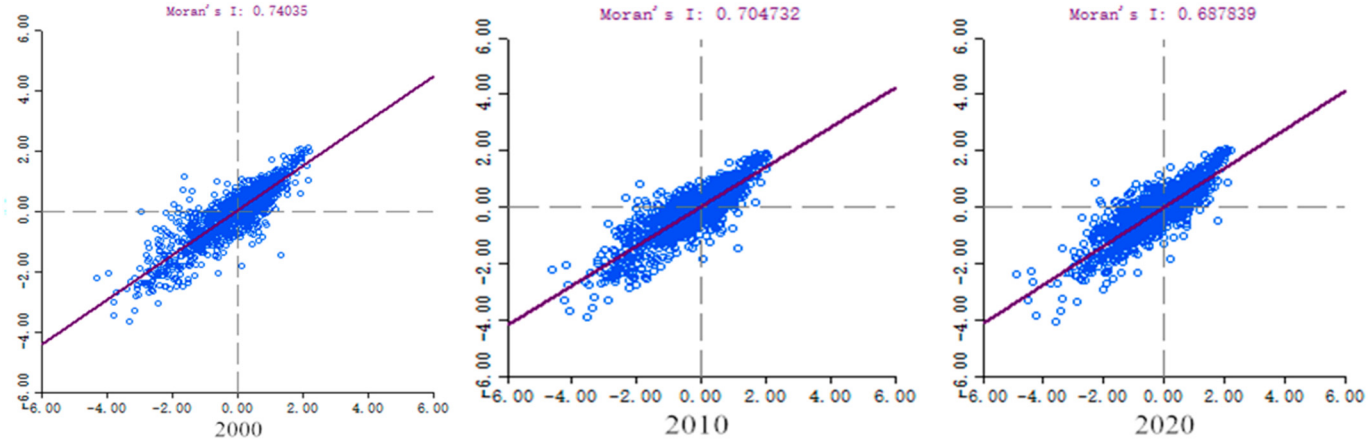

Fig. 6. Moran's *I* scatter diagram of EQ in urban agglomerations in 2000, 2010, and 2020.

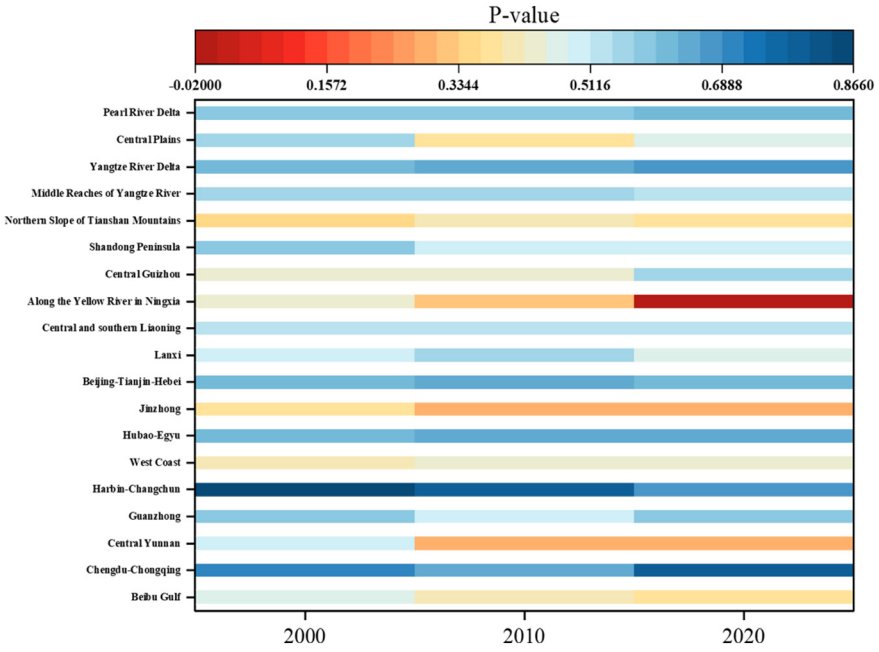

Fig. 7. Moran's *I* index of EQ for urban agglomerations in China in 2000, 2010, and 2020.

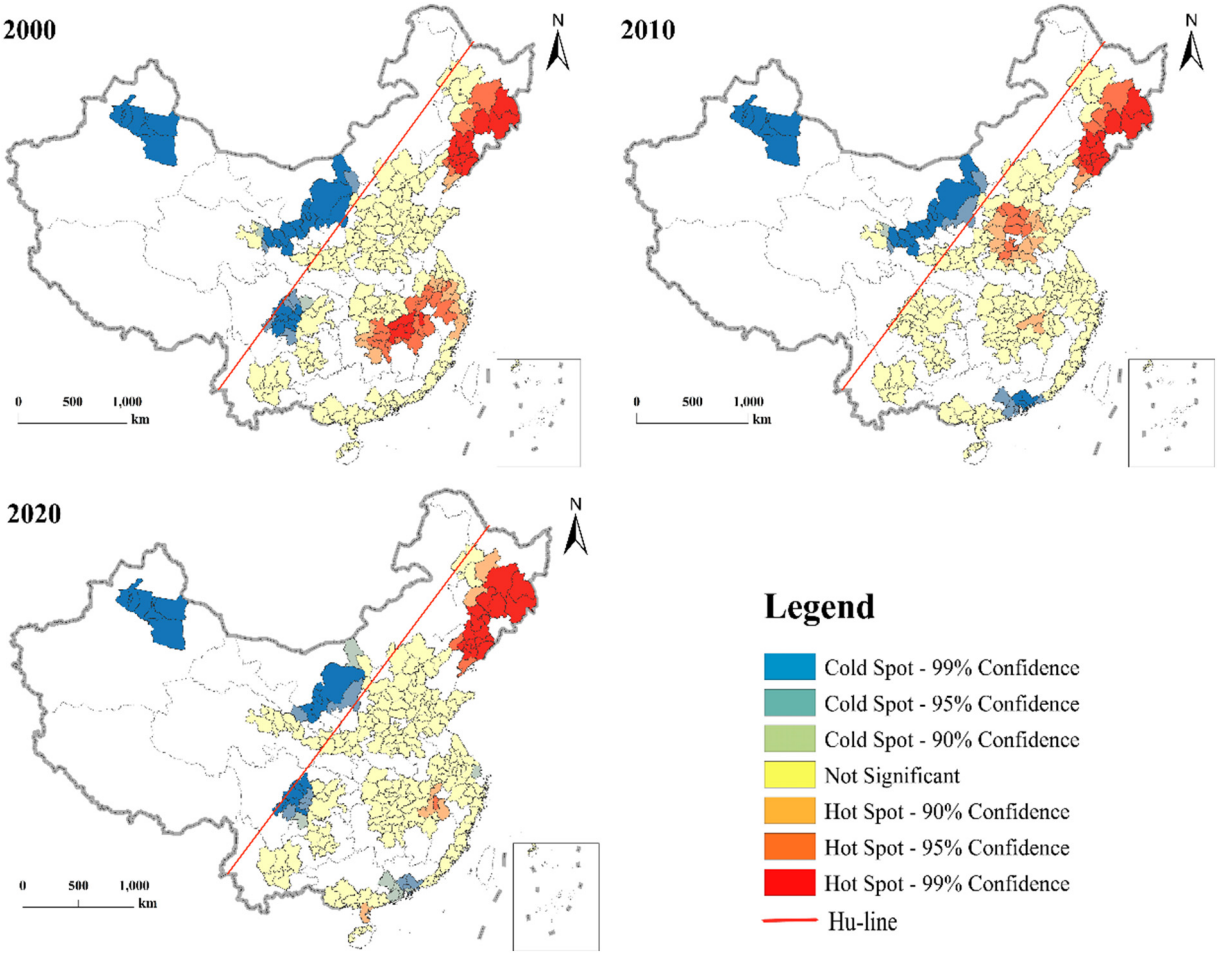

Fig. 8. Spatial and temporal evolutionary patterns of EQ hot spots in 2000, 2010, and 2020.

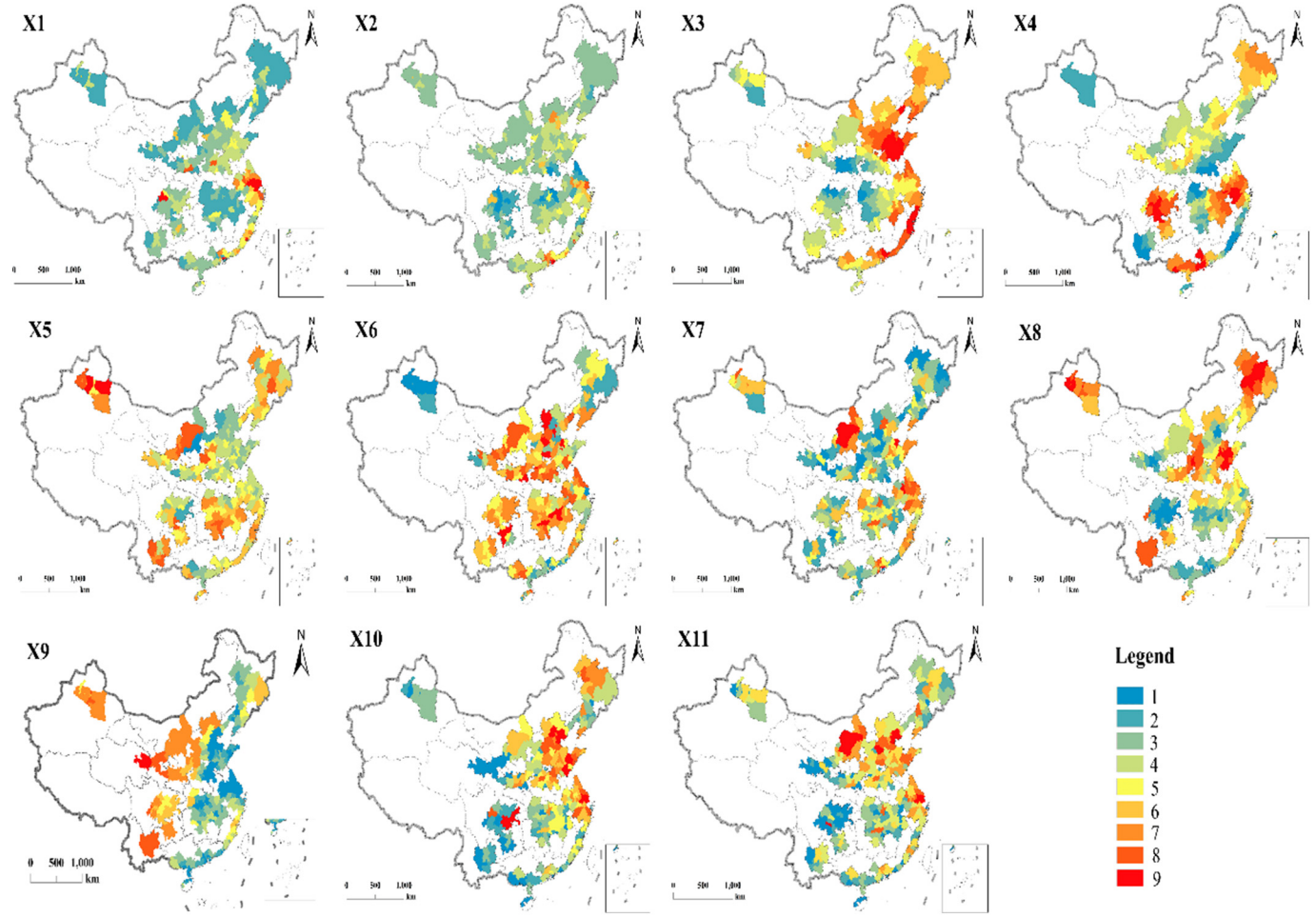

Fig. 9. Spatial distribution of Sen'trend reclassification of driving factors.

EQ in urban agglomerations. The results show that (Table 1) the core drivers being Elevation(X9), Population density (X2), Nighttime light index (X1), Arable land area (X5), Real GDP per capita (X7), Precipitation (X4), Built-up urban area (X10), all of which had an explanatory power >10 % and are the most important drivers of EQ in urban agglomerations. This study analyzed the explanatory power >10 % drivers and the results are as follows.

Elevation influences EQ changes by acting on factors such as runoff (Favis-Mortlock et al., 2022), climate (Zhao et al., 2021), and biology (Zhang et al., 2021a; Zhou et al., 2021). Jiang et al. (2021) concluded that elevation has a greater impact on the intensity of conflict in the natural environment than socioeconomic factors. In the present study, a high driving force for the effect of elevation on EQ.

Urban agglomerations are areas of population and economic concentration where human activity impacts EQ. As an important social indicator, population density is widely used in studies evaluating aspects including urbanization, air quality, and ecology (Borck and Schrauth, 2021; Meng and Han, 2018; Rahman and Alam, 2021). The population density in this study has a high q-value, meaning it is a key driver of EQ.

The nighttime light index reflects, to a certain extent, people's nighttime activities and a region's level of urban development. The nighttime light index has been applied mainly in environmental assessment and urban development (Feng et al., 2020; Kumar et al., 2019; Wang and Liu, 2017; Zhang and Seto, 2011). For example, Ji et al. (2019) found a positive correlation between the nighttime light index and environmental factors. Imhoff et al. (1997) used the nighttime light index to estimate the impact of urban land use on soil resources in the USA.

Arable land area as a type of land use, its change affects the EQ. Arable land area is the basic resource and condition for human to change the surface to satisfaction of survival (Gong et al., 2020). This study found that the change of arable land area has a high driving force on the EQ of urban agglomerations.

Real GDP per capita as an important socio-economic factor has an impact on the ecological environment. Related studies found a correlation between GDP and ecology, ecological carrying capacity, land footprint and waste utilization (Dai et al., 2022; Wu and Zhang, 2021; Chen et al., 2021). This study verified the influence of Real GDP per capita on the EQ of urban agglomerations.

Precipitation plays an important role in regulating surface runoff, improving vegetation cover, and enhancing air quality; within a certain range, it also has a positive effect on the ecological environment (Jiang et al., 2021; Michaelides et al., 2009; Xiao et al., 2021).

Built-up urban area as a type of land use, its change affects the EQ. It is common for scholars to study the ecological impacts of urban area through urban expansion (Hou et al., 2022; Zheng and Qingyun, 2021). This study further confirmed that the development change of the built-up urban area has a driving effect on the change of the EQ.

4.4.3. Master driving analysis of anthropogenic impacts on EQ

The above concluded from the geodetector model that human activities dominate the influence on EQ, except for precipitation and elevation. Therefore, a further importance analysis of the human activity factor was carried out using a stepwise regression model and spatialized mapping (Fig. 10).

Table 1
Factor detection results of GeoDetector.

Code	Index	q statistic
X1	Nighttime light index	0.2007
X2	Population density	0.2258
X3	Temperature	0.0667
X4	Precipitation	0.1482
X5	Arable land area	0.1776
X6	Urbanization level	0.0263
X7	Real GDP per capita	0.1584
X8	PM2.5	0.0802
X9	Elevation	0.2324
X10	Built-up urban area	0.1233
X11	CO_2	0.0379

As shown in Fig. 9b, the results of the stepwise multiple regression model of EQ drivers reveal the important influence of human factors on EQ. As the geographical distribution of urban agglomerations in China has significant spatial differences, the relationship between EQ and anthropogenic factors varies with geographical location, showing significant spatial heterogeneity. In general, Nighttime light index, Arable land area, Population density and real GDP per capita are the main factors affecting EQ, especially nighttime light index and arable land area, which dominate 57.89 % of urban agglomerations. Real GDP per capita dominates 15.78 % of the urban agglomerations, which are located mainly in the eastern part of China.

Overall, there are no single factors driving the changes in EQ, and different drivers play a dominant role in different urban agglomerations (Fig. 10a and b). In China's 19 urban agglomerations, nighttime lighting dominate the change of EQ. The urban agglomerations dominated by nighttime lighting are mainly Harbin–Changchun, Central Yunnan, Central and southern Liaoning, and the Northern slope of the Tianshan Mountains, of which Harbin–Changchun urban agglomeration is the most significant, with a relative contribution of 58.98 %. The real GDP per capita dominated urban agglomerations include Beijing-Tianjin-Hebei, West Coast, and Middle Reaches of Yangtze River, among which Beijing-Tianjin-Hebei urban agglomeration is the most significant, with a relative contribution rate of 34.92 %. The urban agglomerations dominated by population density include Shandong Peninsula, Guanzhong and along the Yellow River in Ningxia, among which Shandong Peninsula urban agglomeration is the most significant, with a relative contribution rate of 43.20 %. The urban agglomerations dominated by arable land mainly include Chengdu-Chongqing, Jinzhong, the Northern slope of the Tianshan Mountains and Pearl River Delta, among which the most significant one is the Chengdu-Chongqing urban agglomeration with a contribution rate of 55.60 %, followed by the urban agglomeration on the northern slope of the Tianshan Mountains with a contribution rate of 23.23 %.

5. Discussion

While urban agglomerations are the carriers of economic and social development, rapid urbanization and industrialization processes have created a series of ecological and environmental problems. This study has attempted to solve the human–land problem of urban agglomeration development by monitoring EQ changes through RS. “Promoting ecological civilization and building a Beautiful China” is an important future development strategy for the country and is also a popular topic of research and exploration in geography. The key to the green, healthy, and sustainable development of Chinese urban agglomerations lies in the scientific identification of the characteristics and patterns of spatial changes in the EQ of those agglomerations and securing an accurate grasp of their driving factors and mechanisms. A further discussion of the following aspects is based on the research in this study.

5.1. Analysis of driving factors of EQ

In the last 20 years, there has been not a single factor driving the change in EQ. In contrast to previous studies (Wu and Zhang, 2021; Zhang et al., 2022), we reveal that different drivers play a dominant role in different urban agglomerations and are expressed spatially. In terms of drivers, extensive research explains that human activities play a positive role in ecological and vegetation improvement. For example, Zhang et al. (2022) indicated the existence of perhaps positive ecological impacts of human activities in studies of urban agglomeration on the northern slope of the Tianshan Mountains. Meanwhile, in a study of vegetation, Guan et al. (2021) found that human activities promoted the greening of vegetation. In this study, we further found that human activities contributed to the improvement of EQ and were particularly typical of the Hubao-Egyu urban agglomeration (Fig. 4 and Fig. 10). Hubao-Egyu urban agglomeration is located in a semi-arid region with severe soil erosion, and the EQ has greatly improved within the last 20 years through a series of active human activities and ecological projects. Grain for green is a national ecological project in the central and western regions in China. This has led to a generally significant improvement relative to urban agglomerations east of the Hu-line, despite the relatively poor EQ base in the northwest.

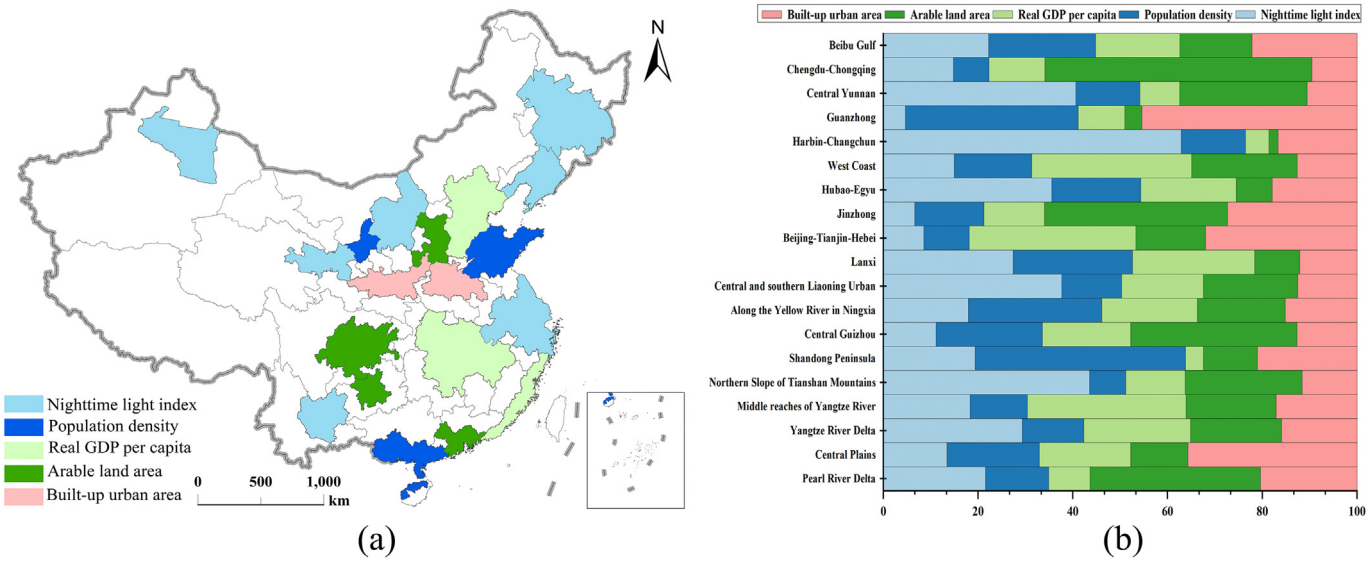

Fig. 10. Spatial distribution of the anthropogenic dominant factor for each urban agglomeration in China.

5.2. Enriching the geographic application of Hu-line

The Hu-line (Hu, 1935), a boundary line used to describe the population differences in China, is embodied in this study and perfectly fits the pattern of east–west divergence in China on a large scale. Scholars widely use it as an important geographic line in analyzing spatial differences, which provides a favorable reference for large-scale spatial studies (Fang et al., 2016b; Kong et al., 2022; Ma et al., 2016; Zhang et al., 2020). In this study, taking the Hu-line as a boundary, the east has fared better than the west (Fig. 4c), eventually identifying the geospatial connection between EQ and the Hu-line, which further enriching the scientific significance of the Hu-line. This also represents a significant geographical finding of the present study.

5.3. Potential applications and limitations

The novelty of this study lies in the fact that it comprehensively reveals the spatial distribution characteristics of long-term serial EQ and the evolution pattern of its spatial agglomeration in urban agglomerations in China, in contrast to previous studies that only considered a single perspective (Yang et al., 2021; Yuan et al., 2021) , and explains the driving factors of EQ in combining GeoDetector and Stepwise multiple regression models, providing a scientific basis for environmental protection policies and the harmonious development of humans and land in urban agglomerations in China. Therefore, the study provides an in-depth scientific analysis of the spatial characteristics and driving mechanisms of EQ in Chinese urban agglomerations based on different scales and elements, thus bridging the gap in this area of research. In terms of data processing, his study used long-term series data for analysis to ensure the scientific and objective nature of the data. At the same time, we adopted multi-year averages in analyzing typical years, which compensated to a certain extent for the defects of RS data subject to environmental interference (Zhou et al., 2019).

There are some limitations to this study, various aspects of this study also require improvement. The evaluation of EQ differed from that used in previous assessments of the ecological risk and ecological footprint, which were overly dependent on socioeconomic data. This also reflects how the evaluation of EQ was limited to the indicators of RS image inversion. The ecological environment and other elements are intertwined and often not the product of the influence of one or two factors alone. Therefore, future studies may consider a more comprehensive selection of RS indices, while further analysis and research are needed to select the driving factors. In addition to the 11 driving factors included in this study, a bold examination of the potential influence of other factors is recommended.

6. Conclusions

Using the GEE platform and MODIS satellite RS data, the EQ of 19 urban agglomerations in China over a recent 21-year period has been dynamically monitored and studied, and the spatial differentiation characteristics and driving mechanisms of EQ of urban agglomerations in China have been explored. The results reveal the following conclusions.

(1) The EQ of the urban agglomerations increased steadily between 2000 and 2020, with the mean value rising from 0.55 to 0.58. Taking the Hu-line as a boundary, the east has fared better than the west. Specifically, the low EQ areas are mainly the urban agglomeration on the northern slope of the Tianshan Mountains, the urban agglomeration along the Yellow River in Ningxia, and the Hubao–Egyu urban agglomeration. The high EQ areas are primarily the Harbin–Changchun, central and southern Liaoning, Jinzhong, and Beibu Gulf urban agglomerations.

(2) During the study period, the EQ of the Central Plains, Central Guizhou, and Central Yunnan urban agglomerations fell slightly, while the EQ of the remaining urban agglomerations improved, accounting for about 84 % of the total number of urban agglomerations.

(3) Moran's *I* index was used to indicate the significant spatial agglomeration characteristics of EQ, with hot spots concentrated mainly in the regions to the east (the Central and southern Liaoning, Harbin–Changchun, Jinzhong, and Central Plains urban agglomerations, etc.) and cold spots concentrated mainly in the regions to the west (the northern slope of the Tianshan Mountains, Hubao–Egyu, Lanxi, and the urban agglomeration along the Yellow River in Ningxia, etc.).

(4) The elevation, population density, nighttime light index, arable land area, real GDP per capita, precipitation, and built-up urban area could explain the spatial changes in China's EQ to a certain extent. The stepwise multiple regression model spatially reveals that the nighttime light index, Built-up urban area and GDP per capita dominate the ecological quality changes of urban agglomerations, accounting for 73.68 % of the total number of urban agglomerations.

This study provides a scientific basis for implementing feasible ecological protection policies in urban agglomerations and provides scientific support for the construction of ecological civilization and the development of human–land harmony, with a view to actively promoting the construction of a “Beautiful China”.

CRediT authorship contribution statement

Lifang Zhang: Conceptualization, Methodology, Software, Investigation, Validation, Writing – review & editing, Writing – original draft. **Chuanglin Fang:** Supervision, Project administration, Formal analysis. **Ruidong Zhao:** Supervision, Validation. **Cong Zhu:** Supervision, Project administration, Validation. **Jingyun Guan:** Methodology, Software, Validation.

Data availability

The data that has been used is confidential.

Declaration of competing interest

The authors declare that they have no known competing financial interests or personal relationships that could have influenced the work reported in this paper.

Acknowledgments

We would like to thank the editor and anonymous reviewers for their valuable comments and suggestions for this paper. This study was funded by the Innovative Research Group Project of the National Natural Science Foundation of China (No. 42121001). We are also grateful to the Data Center for Resources and Environmental Sciences, Chinese Academy of Sciences (RESDC) (http://www.resdc.cn) and National Earth System Science Data Center, National Science & Technology Infrastructure of China (http://www.geodata.cn).

References

Abdulateef, M., Al-Alwan, H., 2020. Assessment of surface urban heat island intensity and its causes in the city of Baghdad. IOP Conf. Ser. Mater. Sci. Eng. 2020 (745), 1–16.
Anselin, L., 1995. Local Indicators of Spatial Association—LISA. Geogr. Anal. 27, 93–115.
Avtar, R., Komolafe, A.A., Kouser, A., Singh, D., Yunus, A.P., Dou, J., et al., 2020. Assessing sustainable development prospects through remote sensing: a review. Remote Sens. Applic. Soc. Environ. 20, 100402.
Azmi, R., Tekouabou Koumetio, C.S., Diop, E.B., Chenal, J., 2021. Exploring the relationship between urban form and land surface temperature (LST) in a semi-arid region case study of Ben Guerir city - Morocco. Environ.Chall. 5, 100229.
Boori, M.S., Choudhary, K., Paringer, R., Kupriyanov, A., 2021. Spatiotemporal ecological vulnerability analysis with statistical correlation based on satellite remote sensing in Samara, Russia. J. Environ. Manag. 285, 112138.
Borck, R., Schrauth, P., 2021. Population density and urban air quality. Reg. Sci. Urban Econ. 86, 103596.
Central People's Government of the People's Republic of China, 2021. The 14th Five-year Plan And the Outline of the Long-term Goals for 2035 (in Chinese).
Chen, Y., Tian, W., Zhou, Q., Shi, T., 2021. Spatiotemporal and driving forces of ecological carrying capacity for high-quality development of 286 cities in China. J. Clean. Prod. 293, 126186.
Chen, Z., Yu, B., Yang, C., Zhou, Y., Yao, S., Qian, X., et al., 2021. An extended time series (2000–2018) of global NPP-VIIRS-like nighttime light data from a cross-sensor calibration. Earth Syst. Sci. Data 13 (3), 889–906.
Cliff, A.D., Ord, J.K., 1982. Spatial processes: models & applications. Q. Rev. 13, 59–60.

Dadashpoor, H., Azizi, P., Moghadasi, M., 2019. Land use change, urbanization, and change in landscape pattern in a metropolitan area. Sci. Total Environ. 655, 707–719.
Dai, Y., Zhang, H., Cheng, J., Jiang, X., Ji, X., Zhu, D., 2022. Whether ecological measures have influenced the environmental Kuznets curve (EKC)? An analysis using land footprint in the Weihe River Basin, China. Ecol. Indic. 139, 108891.
Ding, C., Liu, X., Huang, F., Li, Y., Zou, X., 2017. Onset of drying and dormancy in relation to water dynamics of semi-arid grasslands from MODIS NDWI. Agric. For. Meteorol. 234–235, 22–30.
El-Hattab, M., A, S.M., L, G.E., 2018. Monitoring and assessment of urban heat islands over the Southern region of Cairo Governorate, Egypt. Egypt. J. Remote Sens. Space Sci. 21, 311–323.
Fang, C., 2019. The basic law of the formation and expansion in urban agglomerations. J. Geogr. Sci. 29, 1699–1712.
Fang, C., Liu, H., Li, G., 2016a. International progress and evaluation on interactive coupling effects between urbanization and the eco-environment. J. Geogr. Sci. 26, 1081–1116.
Fang, C., Liu, H., Wang, S., 2021. The coupling curve between urbanization and the eco-environment: China's urban agglomeration as a case study. Ecol. Indic. 130, 108107.
Fang, C., Mao, Q., Ni, P., 2015. The controversy and exploration of scientific selection and gradingdevelopment of Chinese urban agglomeration. Acta Geogr. Sin. 70, 515–527.
Fang, C., Ren, Y., 2017. Analysis of emergy-based metabolic efficiency and environmental pressure on the local coupling and telecoupling between urbanization and the eco-environment in the Beijing-Tianjin-Hebei urban agglomeration. Sci. China Earth Sci. 60, 1083–1097.
Fang, C., Yu, D., 2017. Urban agglomeration: an evolving concept of an emerging phenomenon. Landsc. Urban Plan. 162, 126–136.
Fang, C., Zhou, C., Gu, C., Chen, L., Li, S., 2017. A proposal for the theoretical analysis of the interactive coupled effects between urbanization and the eco-environment in mega-urban agglomerations. J. Geogr. Sci. 27, 1431–1449.
Fang, X., Zou, B., Liu, X., Sternberg, T., Zhai, L., 2016. Satellite-based ground PM2.5 estimation using timely structure adaptive modeling. Remote Sens. Environ. 186, 152–163.
Favis-Mortlock, D., Boardman, J., Foster, I., Shepheard, M., 2022. Comparison of observed and DEM-driven field-to-river routing of flow from eroding fields in an arable lowland catchment. Catena 208, 105737.
Feng, Z., Peng, J., Wu, J., 2020. Using DMSP/OLS nighttime light data and K–means method to identify urban–rural fringe of megacities. Habitat Int. 103, 102227.
Firozjaei, M.K., Kiavarz, M., Homaee, M., Arsanjani, J.J., Alavipanah, S.K., 2021. A novel method to quantify urban surface ecological poorness zone: a case study of several European cities. Sci. Total Environ. 757, 143755.
Gebler, D., Wiegleb, G., Szoszkiewicz, K., 2018. Integrating river hydromorphology and water quality into ecological status modelling by artificial neural networks. Water Res. 139, 395–405.
Getis, A., Ord, J.K., 1996. Local spatial statistics: an overview. In: Longley, P., Batty, M. (Eds.), Spatial Analysis: Modeling in a GIS Environment. Geoinformation International, Cambridge, UK, pp. 261–277.
Gocic, M., Trajkovic, S., 2013. Analysis of changes in meteorological variables using Mann-Kendall and Sen's slope estimator statistical tests in Serbia. Glob. Planet. Chang. 100, 172–182.
Gong, Y., Li, J., Li, Y., 2020. Spatiotemporal characteristics and driving mechanisms of arable land in the Beijing-Tianjin-Hebei region during 1990–2015. Socio Econ. Plan. Sci. 70, 100720.
Groemping, U., 2006. Relative importance for linear regression in R: the package relaimpo. J. Stat. Softw. 17, 1–27.
Guan, J., Yao, J., Li, M., Zheng, J., 2021. Assessing the spatiotemporal evolution of anthropogenic impacts on remotely sensed vegetation dynamics in Xinjiang, China. Remote Sensing.
Guha, S., Govil, H., Dey, A., Gill, N., 2018. Analytical study of land surface temperature with NDVI and NDBI using Landsat 8 OLI and TIRS data in Florence and Naples city, Italy. Eur. J. Remote Sens. 51, 667–678.
Guha, S., Govil, H., Gill, N., Dey, A., 2021. A long-term seasonal analysis on the relationship between LST and NDBI using Landsat data. Quat. Int. 575–576, 249–258.
Guo, M., Li, J., He, H., Xu, J., Jin, Y., 2018. Detecting global vegetation changes using Mann-Kendal (MK) trend test for 1982–2015 time period. Chin. Geogr. Sci. 28, 907–919.
Hou, W., Zhou, W., Li, J., Li, C., 2022. Simulation of the potential impact of urban expansion on regional ecological corridors: a case study of Taiyuan, China. Sustain. Cities Soc. 83, 103933.
Hu, H., 1935. The distribution of population in China. Acta Geogr. Sin. 2, 33–74.
Hu, X., Xu, H., 2018. A new remote sensing index for assessing the spatial heterogeneity in urban ecological quality: a case from Fuzhou City, China. Ecol. Indic. 89, 11–21.
Imhoff, M.L., Lawrence, W.T., Elvidge, C.D., Paul, T., Levine, E., Privalsky, M.V., et al., 1997. Using nighttime DMSP/OLS images of city lights to estimate the impact of urban land use on soil resources in the United States. Remote Sens. Environ. 59, 105–117.
Ji, G., Tian, L., Zhao, J., Yue, Y., Wang, Z., 2019. Detecting spatiotemporal dynamics of PM2.5 emission data in China using DMSP-OLS nighttime stable light data. J. Clean. Prod. 209, 363–370.
Jiang, L., Liu, Y., Wu, S., Yang, C., 2021. Analyzing ecological environment change and associated driving factors in China based on NDVI time series data. Ecol. Indic. 129, 107933.
Jiang, S., Meng, J., Zhu, L., Cheng, H., 2021. Spatial-temporal pattern of land use conflict in China and its multilevel driving mechanisms. Sci. Total Environ. 801, 149697.
Ke, X., Wang, X., Guo, H., Yang, C., Zhou, Q., Mougharbel, A., 2021. Urban ecological security evaluation and spatial correlation research—based on data analysis of 16 cities in Hubei Province of China. J. Clean. Prod. 311, 127613.
Khan, I., Hou, F., Le, H.P., 2021. The impact of natural resources, energy consumption, and population growth on environmental quality: fresh evidence from the United States of America. Sci. Total Environ. 754, 142222.
Kong, X., Fu, M., Zhao, X., Wang, J., Jiang, P., 2022. Ecological effects of land-use change on two sides of the Hu Huanyong Line in China. Land Use Policy 113, 105895.
Kumar, P., Sajjad, H., Joshi, P.K., Elvidge, C.D., Rehman, S., Chaudhary, B.S., et al., 2019. Modeling the luminous intensity of Beijing, China using DMSP-OLS night-time lights series data for estimating population density. Phys. Chem. Earth A/B/C 109, 31–39.
Lemoine-Rodríguez, R., Inostroza, L., Zepp, H., 2022. Does urban climate follow urban form? Analyzing intraurban LST trajectories versus urban form trends in 3 cities with different background climates. Sci. Total Environ. 830, 154570.
Liu, Y., Li, Z., Chen, Y., Li, Y., Li, H., Xia, Q., et al., 2022. Evaluation of consistency among three NDVI products applied to High Mountain Asia in 2000–2015. Remote Sens. Environ. 269, 112821.
Luo, W., Jasiewicz, J., Stepinski, T., Wang, J., Xu, C., Cang, X., 2016. Spatial association between dissection density and environmental factors over the entire conterminous United States. Geophys. Res. Lett. 43, 692–700.
Mann, H.B., 1945. Non-parametric tests against trend. Econometrica 13, 245–259.
Ma, T., Li, C., Lu, Z., 2016. Geographical environment determinism for discovery of mineral deposits. J. Geochem. Explor. 168, 163–168.
Meng, X., Han, J., 2018. Roads, economy, population density, and CO2: a city-scaled causality analysis. Resour. Conserv. Recycl. 128, 508–515.
Michaelides, S., Levizzani, V., Anagnostou, E., Bauer, P., Kasparis, T., Lane, J.E., 2009. Precipitation: measurement, remote sensing, climatology and modeling. Atmos. Res. 94, 512–533.
Moran, P.A.P., 1950. Notes on continuous stochastic phenomena. Biometrika 37, 17–23.
Ministry of Ecology and Environment of the People's Republic of China, 2020. Protecting the Environment is Established as a Basic National Policy (in Chinese).
National Development and Reform Commission, 2021. Interpretation of the Outline of the 14th Five-year Plan: Continuous Improvement of Environmental Quality (in Chinese).
Pan, N., Wang, S., Wei, F., Shen, M., Fu, B., 2021. Inconsistent changes in NPP and LAI determined from the parabolic LAI versus NPP relationship. Ecol. Indic. 131, 108134.
Peng, S., Ding, Y., Liu, W., Li, Z., 2019. 1 km monthly temperature and precipitation dataset for China from 1901 to 2017. Earth Syst. Sci. Data 11, 1931–1946.
Qiu, M., Yang, Z., Zuo, Q., Wu, Q., Jiang, L., Zhang, Z., et al., 2021. Evaluation on the relevance of regional urbanization and ecological security in the nine provinces along the Yellow River, China. Ecol. Indic. 132, 108346.
Rahman, M.M., Alam, K., 2021. Clean energy, population density, urbanization and environmental pollution nexus: evidence from Bangladesh. Renew. Energy 172, 1063–1072.
Rikimaru, A., Partha Sarathi, R., Miyatake, S., 2002. Tropical forest cover density mapping. Trop. Ecol. 43, 39–47.
Sen, P.K., 1968. Estimates of the regression coefficient based on Kendall's tau. J. Am. Stat. Assoc. 63, 1379–1389.
Shan, W., Jin, X., Ren, J., Wang, Y., Xu, Z., Fan, Y., et al., 2019. Ecological environment quality assessment based on remote sensing data for land consolidation. J. Clean. Prod. 239, 118126.
Shan, Y., Huang, Q., Guan, D., Hubacek, K., 2020. China CO2 emission accounts 2016–2017. Sci. Data 7, 54.
Shao, Z., Ding, L., Li, D., Altan, O., Huq, M.E., Li, C., 2020. Exploring the relationship between urbanization and ecological environment using remote sensing images and statistical data: a case study in the Yangtze River Delta, China. Sustainability 12.
Singh, P., Kikon, N., Verma, P., 2017. Impact of land use change and urbanization on urban heat island in Lucknow city, Central India. A remote sensing based estimate. Sustain. Cities Soc. 32, 100–114.
Subhanil, G., Himanshu, G., Prabhat, D., 2019. Analytical study of seasonal variability in land surface temperature with normalized difference vegetation index, normalized difference water index, normalized difference built-up index, and normalized multiband drought index. J. Appl. Remote. Sens. 13, 1–16.
The 18th National Congress of the Communist Party of China, 2012. "Beautiful China" Draws a New Picture: Deputies to the 18th National Congress Talk About Ecological Civilization Construction (in Chinese).
Tang, P., Huang, J., Zhou, H., Fang, C., Zhan, Y., Huang, W., 2021. Local and telecoupling coordination degree model of urbanization and the eco-environment based on RS and GIS: a case study in the Wuhan urban agglomeration. Sustain. Cities Soc. 75, 103405.
Todd, S., Hoffer, R., 1998. Responses of spectral indices to variations in vegetation cover and soil background. Photogramm. Eng. Remote 64, 915–922.
Wang, C., Qo, Jiang, Shao, Y., Sun, S., Xiao, L., Guo, J., 2019. Ecological environment assessment based on land use simulation: a case study in the Heihe River Basin. Sci. Total Environ. 697, 133928.
Wang, J., Xu, C., 2017. Geodetector: principle and prospective. Acta Geogr. Sin. 72, 116–134 (in Chinese).
Wang, J., Li, X., Christakos, G., Liao, Y., Zhang, T., Gu, X., et al., 2010. Geographical detectors-based health risk assessment and its application in the neural tube defects study of the Heshun Region, China. Int. J. Geogr. Inf. Sci. 24, 107–127.
Wang, S., Liu, X., 2017. China's city-level energy-related CO2 emissions: spatiotemporal patterns and driving forces. Appl. Energy 200, 204–214.
Wang, Z., Li, J., Liang, L., 2022. Ecological risk in the Tibetan Plateau and influencing urbanization factors. Environ. Chall. 6, 100445.
Wei, J., Li, Z., Lyapustin, A., Sun, L., Peng, Y., Xue, W., Su, T., Cribb, M., 2021. Reconstructing 1-km-resolution high-quality PM2.5 data records from 2000 to 2018 in China: spatiotemporal variations and policy implications. Remote Sens. Environ. 252, 112136.
Wu, X., Zhang, H., 2021. Evaluation of ecological environmental quality and factor explanatory power analysis in western Chongqing, China. Ecol. Indic. 132, 108311.
Xiao, D., Chen, Y., He, X., Xu, Z., Hosseini Bai, S., Zhang, W., et al., 2021. Temperature and precipitation significantly influence the interactions between arbuscular mycorrhizal fungi and diazotrophs in karst ecosystems. For. Ecol. Manag. 497, 119464.
Xie, H., Yao, G., Liu, G., 2015. Spatial evaluation of the ecological importance based on GIS for environmental management: a case study in Xingguo county of China. Ecol. Indic. 51, 3–12.
Xiong, Y., Xu, W., Lu, N., Huang, S., Wu, C., Wang, L., et al., 2021. Assessment of spatial–temporal changes of ecological environment quality based on RSEI and GEE: a case study in Erhai Lake Basin, Yunnan province, China. Ecol. Indic. 125, 107518.

Xu, D., Yang, F., Yu, L., Zhou, Y., Li, H., Ma, J., et al., 2021. Quantization of the coupling mechanism between eco-environmental quality and urbanization from multisource remote sensing data. J. Clean. Prod. 321, 128948.
Xu, H., 2008. A new index for delineating built-up land features in satellite imagery. Int. J. Remote Sens. 29, 4269–4276.
Xu, H., 2013. A remote sensing index for assessment of regional ecological changes. China Environ. Sci. 33, 889–897 (in Chinese).
Xu, H., Wang, Y., Guan, H., Shi, T., Hu, X., 2019. Detecting ecological changes with a Remote Sensing Based Ecological Index (RSEI) produced time series and change vector analysis. Remote Sens. 11.
Yang, J., Huang, X., 2021. The 30 m annual land cover datasets and its dynamics in China from 1990 to 2020 (1.0.0). Zenodo 13 (8).
Yang, X., Meng, F., Fu, P., Zhang, Y., Liu, Y., 2021. Spatiotemporal change and driving factors of the Eco-Environment quality in the Yangtze River Basin from 2001 to 2019. Ecol. Indic. 131, 108214.
Yao, J., Xu, P., Huang, Z., 2021. Impact of urbanization on ecological efficiency in China: an empirical analysis based on provincial panel data. Ecol. Indic. 129, 107827.
Yuan, B., Fu, L., Zou, Y., Zhang, S., Chen, X., Li, F., Deng, Z., Xie, Y., 2021. Spatiotemporal change detection of ecological quality and the associated affecting factors in Dongting Lake Basin, based on RSEI. J. Clean. Prod. 302, 126995.
Yurui, L., Xuanchang, Z., Zhi, C., Zhengjia, L., Zhi, L., Yansui, L., 2021. Towards the progress of ecological restoration and economic development in China's Loess Plateau and strategy for more sustainable development. Sci. Total Environ. 756, 143676.
Zhang, L., Fang, C., Zhu, C., Gao, Q., 2022. Ecosystem service trade-offs and identification of eco-optimal regions in urban agglomerations in arid regions of China. J. Clean. Prod. 373, 133823.
Zhang, M., Sun, X., Wang, W., 2020. Study on the effect of environmental regulations and industrial structure on haze pollution in China from the dual perspective of independence and linkage. J. Clean. Prod. 256, 120748.
Zhang, Q., Seto, K.C., 2011. Mapping urbanization dynamics at regional and global scales using multi-temporal DMSP/OLS nighttime light data. Remote Sens. Environ. 115, 2320–2329.
Zhang, X., Schaaf, C.B., Friedl, M.A., Strahler, A.H., Feng, G., Hodges, J.C.F., 2002. MODIS tasseled cap transformation and its utility. IEEE International Geoscience And Remote Sensing Symposium. 2. IGARSS '02. IEEE International, pp. 1063–1065.
Zhang, Y., Ji, L., Yang, L., 2021a. Abundance and diversity of soil nematode community at different altitudes in cold-temperate montane forests in northeast China. Glob. Ecol. Conserv. 29, e01717.
Zhang, Y., She, J., Long, X., Zhang, M., 2022. Spatio-temporal evolution and driving factors of eco-environmental quality based on RSEI in Chang-Zhu-Tan metropolitan circle, central China. Ecol. Indic. 144, 109436.
Zhang, Y., Migliavacca, M., Penuelas, J., Ju, W., 2021b. Advances in hyperspectral remote sensing of vegetation traits and functions. Remote Sens. Environ. 252, 112121.
Zhao, Y.F., Wang, X., Jiang, S.L., Zhou, X.H., Liu, H.Y., Xiao, J.J., et al., 2021. Climate and geochemistry interactions at different altitudes influence soil organic carbon turnover times in alpine grasslands. Agric. Ecosyst. Environ. 320, 107591.
Zheng, Z., Qingyun, H., 2021. Spatio-temporal evaluation of the urban agglomeration expansion in the middle reaches of the Yangtze River and its impact on ecological lands. Sci. Total Environ. 790, 148150.
Zheng, Z., Wu, Z., Chen, Y., Guo, C., Marinello, F., 2022. Instability of remote sensing based ecological index (RSEI) and its improvement for time series analysis. Sci. Total Environ. 814, 152595.
Zheng, Z., Wu, Z., Chen, Y., Yang, Z., Marinello, F., 2020. Exploration of eco-environment and urbanization changes in coastal zones: a case study in China over the past 20 years. Ecol. Indic. 119, 106847.
Zhou, L., Zhou, C., Yang, F., Che, L., Wang, B., Sun, D., 2019. Spatio-temporal evolution and the influencing factors of PM2.5 in China between 2000 and 2015. J. Geogr. Sci. 29, 253–270.
Zhou, P., Huang, J.-G., Liang, H., Rossi, S., Bergeron, Y., Shishov, V.V., et al., 2021. Radial growth of Larix sibirica was more sensitive to climate at low than high altitudes in the Altai Mountains,China. Agric. For. Meteorol. 304–305, 108392.